The effect of longitudinal density gradient on electron plasma wake field acceleration

David Tsiklauri
School of Physics and Astronomy, Queen Mary University of London, London, E1 4NS, United Kingdom

arXiv:1606.00367v1 [physics.plasm-ph] 1 Jun 2016

Three-, two- and one-dimensional, particle-in-cell, fully electromagnetic simulations of electron plasma wake field acceleration in the blow out regime are presented. Earlier results are extended by (i) studying the effect of longitudinal density gradient; (ii) avoiding use of co-moving simulation box; (iii) inclusion of ion motion; and (iv) studying fully electromagnetic plasma wake fields. It is established that injecting driving and trailing electron bunches into a positive density gradient of ten-fold increasing density over 10 cm long Lithium vapor plasma, results in spatially more compact and three times larger, compared to the uniform density case, electric fields (-6.4×10^{10} V/m), leading to acceleration of the trailing bunch up to 24.4 GeV (starting from initial 20.4 GeV), with an energy transfer efficiencies from leading to trailing bunch of 75 percent. In the uniform density case -2.5×10^{10} V/m wake is created leading to acceleration of the trailing bunch up to 22.4 GeV, with an energy transfer efficiencies of 65 percent. It is also established that injecting the electron bunches into a negative density gradient of ten-fold decreasing density over 10 cm long plasma, results in spatially more spread and two-and-half smaller electric fields (-1.0×10^{10} V/m), leading to a weaker acceleration of the trailing bunch up to 21.4 GeV, with an energy transfer efficiencies of 45 percent. It is shown that two-dimensional simulation results are substantially different from the three-dimensional ones, showing only 10 percent efficiency of trailing bunch acceleration, while in one-dimensional case no acceleration is seen. Inclusion of ion motions into consideration shows that in the plasma wake ion number density can increase over few times the background value. We also show that transverse electromagnetic fields in plasma wake are of the same order as the longitudinal (electrostatic) ones.

I. INTRODUCTION

Conventional particle accelerators have an accelerating gradient of tens of MV/m. The limit is set by the radio frequency (RF) breakdown phenomenon, when large electric field in the accelerator cavities causes accelerator to be effectively short-circuited. It is known that when electric field exceeds a threshold value, the Kilpatrick limit, no matter how good the vacuum in the accelerator tube is, there will be a RF breakdown and nearly all of the RF power is absorbed [4]. Thus the beam receives little or no acceleration in the cavity. Novel accelerator concepts that have a promise to overcome the difficulties of conventional particle accelerators include plasma wake field acceleration (PWFA), amongst a number of other concepts such as fixed-field alternating-gradient accelerators, dielectric wall accelerators, and dielectric laser accelerators. Plasma wake field acceleration usually refers to an acceleration of particles through the generation of strong electric fields from charged particle motion in plasma. Generally a distinction is drawn between beam-driven PWFA and laser-driven plasma wake field acceleration (LWFA). The advantage of accelerators based on plasmas, is that they can sustain electric fields up to tens of GV/m, without electric short-circuiting, and have a potential to be a smaller and cheaper than the conventional accelerators. An electrostatic wave in plasma, co-propagating with a charged-particle bunch/beam, can keep the bunch in a high-field region over a path of a meter or more, thus transferring substantial amounts of energy to the particles in a compact space. However, the precision engineering is required to accelerate particles efficiently and uniformly and this has been a challenge.

Recently authors of Ref.[5] have taken a leap forward in PWFA. In their plasma wake field accelerator, the plasma wave is created by a 20-GeV electron bunch from SLAC's linac. A second bunch of equally energetic electrons follows close behind. With SLAC's purpose-built Facility for Advanced Accelerator Experimental Tests (FACET) [2], authors could place the trailing bunch at just the right spot in the plasma wave to increase the bunch energy by 1.6 GeV over just 30 cm of plasma. In Ref.[5] 3D particle-in-cell (PIC) simulations with resolution of 512^3 spatial grids of a plasma wake field interaction with beam were also carried out. They established that the drive bunch clears away the plasma electrons, leaving a region of strong but inhomogeneous electric field in its wake. If the trailing bunch is large enough and positioned in the right spot, it can flatten the electric field so that the trailing bunch is uniformly accelerated [5]. Thus, PWFA is an attractive concept to achieve the acceleration of about 74 pC of charge contained in the core of the trailing bunch in an accelerating gradient of about 4.4 GV/m. These core particles gain about 1.6 GeV of energy per particle, with a final energy spread as low as 0.7 % (2.0 % on average), and an energy-transfer efficiency from the wake to the bunch that can exceed 30 % (17.7 % on average). This acceleration of a distinct bunch of electrons containing a substantial charge and having a small energy spread with both high accelerating gradient and high energy-transfer efficiency represents a milestone in the development of PWFA into a compact and affordable accelerator technology. Despite these ground breaking advances there is a room for improvements: (i) An energy gain by the core electron bunch of about 10% can potentially be improved. (ii) From the 800 pC that

started out in the trailing bunch, only 74 pC remained in the accelerated core. Better preservation of the beam is a priority for future work. (iii) Previous numerical simulations of PWFA have predicted the hosing instability to be disrupting the efficient acceleration. This has not been observed in the experiments [2, 5, 6]. Further work is needed to settle this issue.

Recently an interesting opportunity has been explored by Ref.[8]. In this work a beam of accelerated electrons was injected into a magnetized, Maxwellian, homogeneous, and inhomogeneous background plasma. It was established that in the case of increasing density along the path of an electron beam wave-particle resonant interaction of Langmuir waves (the same type of wave as in PWFA) with the beam electrons leads to an efficient particle acceleration. This is because Langmuir waves drift to smaller wave-numbers, k, allowing them to increase their phase speed, $V_{ph} = \omega/k$, and, therefore, being subject to absorption by faster electrons. This is a novel aspect and has not been yet explored in the PWFA context. Therefore the main motivation for this study is to explore the effect of longitudinal density gradient on electron plasma wake field acceleration.

Section II presents the model and results. Section III summaries the main findings.

II. THE MODEL AND RESULTS

The simulation is carried out using EPOCH, a fully electromagnetic (EM), relativistic PIC code [1]. EPOCH is freely available for download from `https://cfsa-pmw.warwick.ac.uk`. We carried out seven numerical runs in total. Three runs with uniform, increasing (positive) and negative (decreasing) density gradients in three and two spatial dimensions (3D and 2D), and one run with uniform density in one spatial dimension (1D). See supplemental material at `http://ph.qmul.ac.uk/~tsiklauri/pwfa1` for the seven input parameter files used in the simulation. The simulation parameters are similar to SLAC's FACET experiment [2] and to Ref.[5]. In uniform density runs plasma number density is set to $n_e = n_i = n_0 = 5 \times 10^{22}$ m^{-3}. As described in Ref.[7], plasma source in such experiments as FACET is produced by photo-ionization of Lithium vapor contained in heat-pipe oven. We set similar parameters: Lithium plasma temperature of $T = 2.5 \times 10^4$ K and mass ratio of $m_i/m_e = 12853.1$. Both electron bunch temperatures are also set to $T_b = 2.5 \times 10^4$ K, producing a very narrow energy/velocity distribution spread (see the two bottom panels in Fig.3). The simulations domain is split into $n_x \times n_y \times n_z = 7992 \times 24 \times 24$ grid cells in x-, y- and z-directions, respectively. The actual simulated domain size is within following bounds $0 \le x_{max} \le 10.529748$ cm and $0 \le y_{max}, z_{max} \le 234.229$ μm. This implies the unit grid size in x-direction is $270\lambda_D$, while in y- and z-directions grid size is $200\lambda_D$. Here $\lambda_D = v_{th,e}/\omega_{pe} = 0.048798$ μm is the Debye length, with $v_{th,e}/c = \sqrt{k_B T/m_e}/c = 0.00205332$ being electron thermal speed and $\omega_{pe} = 1.2614673 \times 10^{13}$ Hz rad is the plasma frequency. It maybe counter-intuitive that simulations with under-resolved Debye length are valid. The validity is two-fold: (i) the typical total energy error in our simulations (see e.g. Fig.4) is 0.00065; (ii) the experimentally validated simulation results of Ref.[5] use 512^3 grids, which means their grid sizes in y- and z-directions are under-resolved by a factor of $4918/512 = 9.6$ (this is because $4918\lambda_D$ fit into their y- and z-direction domain sizes of 240 μm). Thus it is acceptable to under-resolve Debye length in such simulations as the electron beams are in blow out regime. This is understandable, because in plasma PIC simulation unscreened electric fields, within the under-resolved Debye sphere, lead to onset of numerical instabilities that result in what is known as "numerical heating". The latter manifests itself through the total energy increase. On contrary, because finite differencing always leads to a numerical diffusion, the total energy must decrease in time. When it increases in time this means that numerical instability is triggered. However, if the total energy error (see e.g. Fig.4) is 0.00065 (i.e. 0.065 percent) such simulations are acceptable.

In the positive density gradient runs plasma (both background electrons and ions) number densities vary with distance x, in metres, as:

$$n_{PG}(x) = n_0 \left(1.0 + \frac{9.0x}{x_{max}}\right) \left[\tanh\left(\frac{x}{0.005x_{max}}\right) + \tanh\left(-\frac{x - x_{max}}{0.005x_{max}}\right) - 1.0\right]. \quad (1)$$

This implies that the density rises from zero to n_0 over a length of 1 mm, then keeps linearly rising to $10n_0$ and in the final 1 mm of the domain it falls to zero again. In equations 1-4 the distances are quoted in metres.

In the negative density gradient runs plasma number densities vary with distance x as:

$$n_{NG}(x) = n_0 \left(1.0 - \frac{0.9x}{x_{max}}\right) \left[\tanh\left(\frac{x}{0.005x_{max}}\right) + \tanh\left(-\frac{x - x_{max}}{0.005x_{max}}\right) - 1.0\right]. \quad (2)$$

This implies that the density rises from zero to n_0 over a length of 1 mm, then keeps linearly decreasing to $0.1n_0$ and in the final 1 mm of the domain it falls to zero again. Such background density profiles (equations 1 and 2) allow to use periodic boundary conditions, which we use in all our numerical simulations.

The trailing and driving electron bunches have the number densities as follows:

$$n_T(x) = n_0 \exp\left[-\frac{(x - 10.0c/\omega_{pe})^2}{2.0(2.0c/\omega_{pe})^2}\right] \exp\left[-\frac{(y - y_{max}/2.0)^2}{2.0(c/\omega_{pe})^2}\right] \exp\left[-\frac{(z - z_{max}/2.0)^2}{2.0(c/\omega_{pe})^2}\right], \quad (3)$$

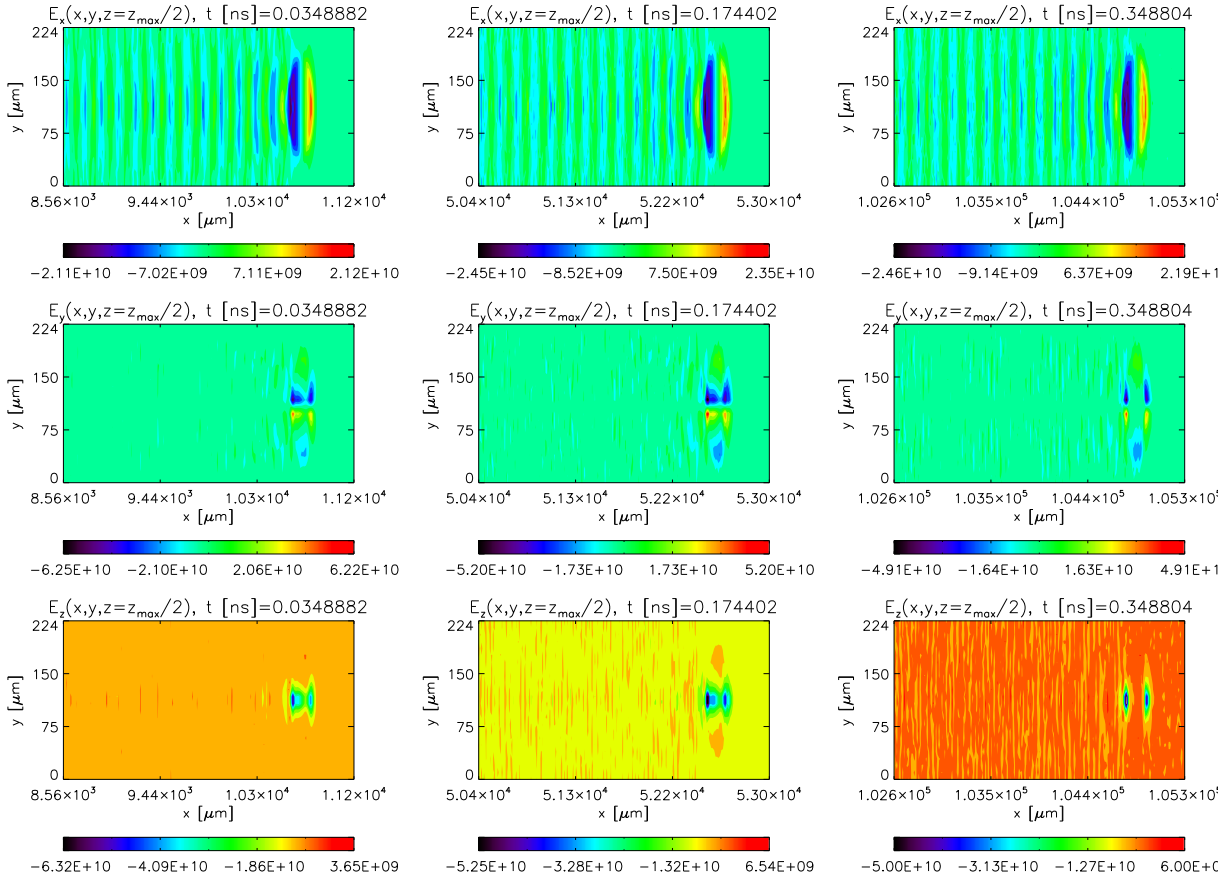

FIG. 1: Contour plots of electric field x- (top row), y- (middle row) and z- (bottom row) components in (x,y) plane (cut through $z = z_{max}/2$) at different time instants corresponding to 1/10th, half and the final simulations times. The fields on color bars are quoted in V/m and time at the top of each panel is in nano-seconds. The data is for uniform density 3D run.

$$n_D(x) = 2.5 n_0 \exp\left[-\frac{(x - 15.7c/\omega_{pe})^2}{2.0(c/\omega_{pe})^2}\right] \exp\left[-\frac{(y - y_{max}/2.0)^2}{2.0(c/\omega_{pe})^2}\right] \exp\left[-\frac{(z - z_{max}/2.0)^2}{2.0(c/\omega_{pe})^2}\right]. \quad (4)$$

These expressions imply that trailing bunch is centered on $10.0c/\omega_{pe} = 237.65183$ μm, has x-length of $\sigma_x = 2.0c/\omega_{pe} = 47.530365$ μm, while driving bunch is 2.5 denser than both the background and trailing bunch, is centered on $15.7c/\omega_{pe} = 373.11337$ μm and has x-length of $\sigma_x = c/\omega_{pe} = 23.765183$ μm. The distance between the trailing and driving bunches is $5.7c/\omega_{pe} = 135.46154$ μm. This is the crucial parameter because the typical measured and simulated longitudinal scale of the plasma wake field for the density of $n_0 = 5 \times 10^{22}$ m^{-3} is about 200 μm [5]. Thus the trailing bunch should lag behind the driving bunch by lesser than this length. Our bunch separation of ≈ 135 μm sits comfortably within this range. Both electron bunches have y- and z-lengths of $\sigma_{y,z} = c/\omega_{pe} = 23.765183$ μm and are centered on $y_{max}/2 = z_{max}/2 = 117.11432$ μm.

We set both electron bunch initial momenta to $p_x = p_0 = 1.087587 \times 10^{-17}$ kg m s^{-1} (note that $p_x/(m_e c) = 39825.1$), which corresponds to an initial energy of $E_0 = 20.35$ GeV. There are four plasma species present in all numerical simulations. In the 3D runs we have $73,654,272$ particles for each of the four species i.e. roughly 3×10^8 particles in total. In the 2D runs we have $34,525,440$ particles for each of the four species, while in 1D each species have $1,438,560$ particles. The three dimensional runs take about 27 hours on 192 computing cores, using Intel Xeon E5-2650 16-core 2.6GHz CPUs with 64 Gb of random access memory (RAM). These use $n_x \times n_y \times n_z = 12 \times 4 \times 4$ domain decomposition for optimal code performance, particularly alleviating the particle dynamical load balancing overheads. The bottle neck for this type of simulations is the amount of RAM on each of the 16-core nodes. With twelve nodes the total of $12 \times 64 = 768$ Gb of RAM was available. Background electrons and ions are distributed evenly over 192 cores, but driving and trailing bunches are very localized and move with nearly at the speed of light. This puts tight limitation on number of particles that can be used to resolve bunch electrons because both bunches must fit

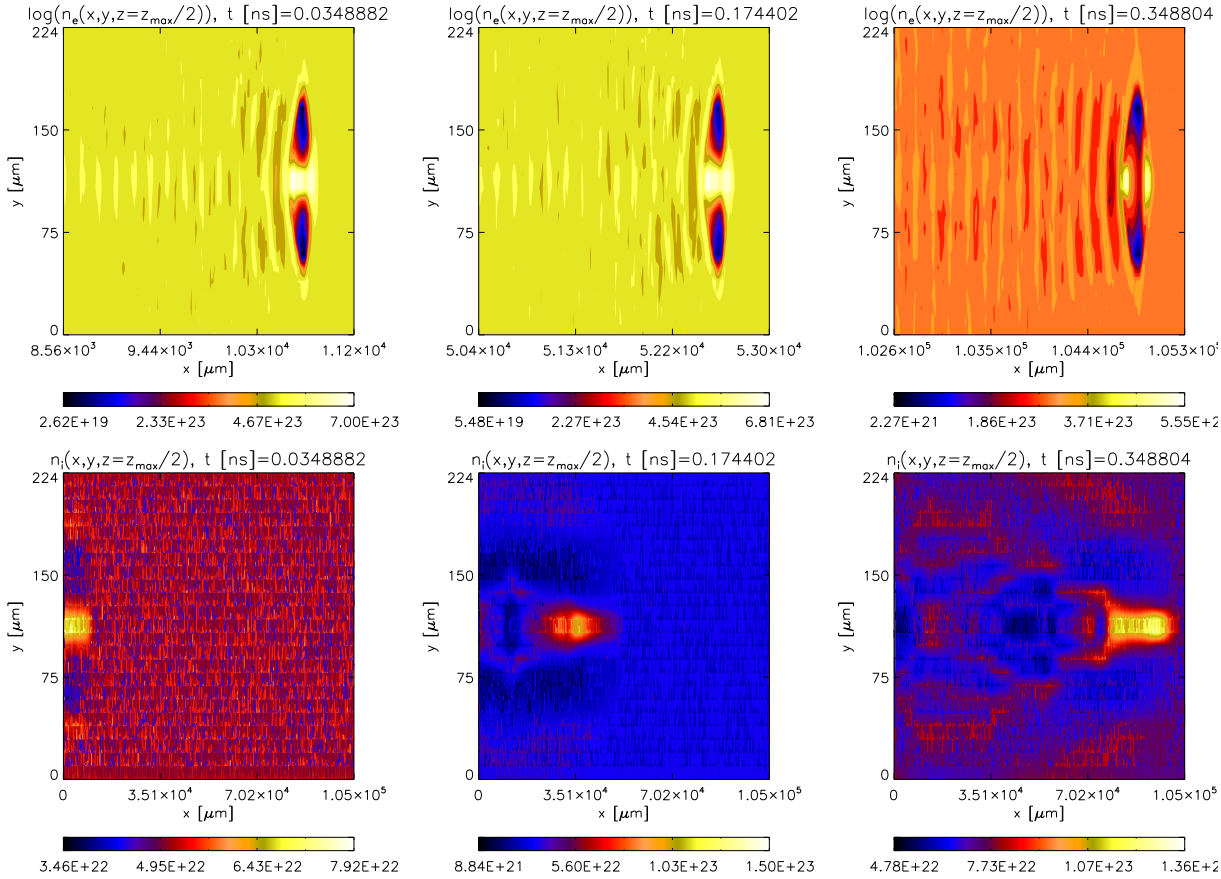

FIG. 2: Contour plots of logarithm of electron (top row) and ion (bottom row) in (x,y) plane (cut through $z = z_{max}/2$) at different time instants corresponding to 1/10th, half and the final simulations times. The number densities on color bars are quoted in m^{-3} and time at the top of each panel is in nano-seconds. The data is for uniform density 3D run.

computationally on the 64 Gb RAM compute nodes they fly through.

Ref.[5] used QuickPIC [3] fully relativistic, 3D, particle-in-cell model bespoke for simulating plasma and laser wake field acceleration. QuickPIC is based on the quasi-static approximation, which reduces a fully 3D, EM field solve and particle push into two spatial dimensions. This is achieved by calculating the plasma wake based on the assumption of drive beam and/or laser not evolving during the time it takes for it to pass a plasma particle. The complete EM fields of the plasma wake and its associated index of refraction are then used to evolve the drive beam and/or laser using large time steps. Ref.[3] suggests that the algorithm reduces the computation time by 2 to 3 orders of magnitude without loss of accuracy. In our numerical work the EPOCH code [1] is used which is free from simplifying assumptions of QuickPIC, i.e. it is an explicit, fully electromagnetic, relativistic PIC code. Thus, it is interesting to compare the findings of both approaches.

A. 3D uniform density case

Fig.1 top row shows contour plots of electric field E_x component at three times. We see that the yellow half-ellipse, representing positive $E_x \approx 2.2\times10^{10}$ V/m plasma wake remains nearly constant in shape and its amplitude and travelled correct distances of $0.0349 \times 10^{-9} \times c = 10463$ μm, $0.1744 \times 10^{-9} \times c = 52283$ μm and $0.3488 \times 10^{-9} \times c = 104567$ μm within the corresponding times. We also see that negative, $E_x \approx -2.5 \times 10^{10}$ V/m, the dark blue half-ellipse, closely follows the yellow one. It is this region of negative E_x that accelerates the trailing bunch. Ref.[5] has not presented the transverse EM field dynamics. We show this in the middle and lower rows of Fig.1. In Fig.1 middle row shows contour plots of electric field E_y component at three times. We see that E_y has quadrupolar structure with two positive peaks on the right side and two negative dips on the left side of the drive bunch path. The amplitudes of the quadrupolar $E_y \approx \pm5\times10^{10}$ V/m and are co-located (across x-position) with E_x positive and negative electrostatic wakes. Fig.1 lower row shows contour plots of elec-

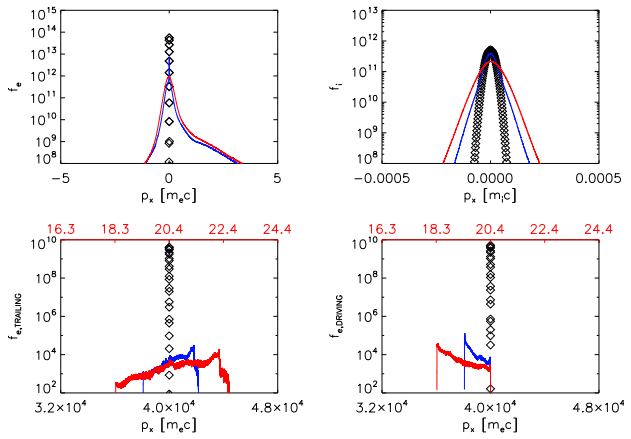

FIG. 3: Electron, ion, trailing and driving electron bunch distribution functions at different times: open diamonds correspond to $t = 0$, while blue and red curves to the half and the final simulations times, respectively. x-axis are momenta quoted in the units of relevant species mass times speed of light. In the bottom row top x-axis is quoted in GeV to aid eye visualizing of trailing bunch acceleration and driving bunch deceleration processes. The data is for uniform density 3D run.

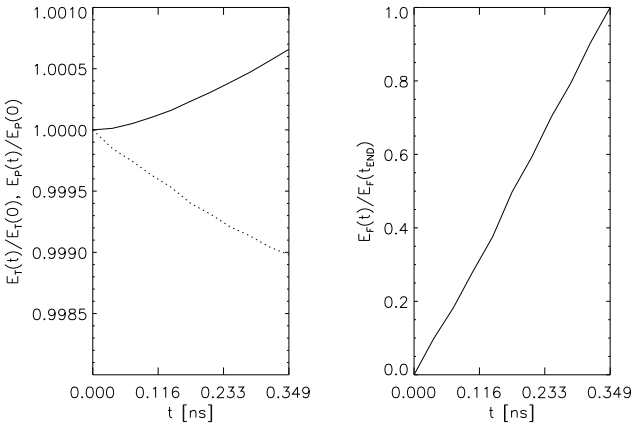

FIG. 4: Left panel's solid and dashed curves are the total (particles plus EM fields) and particle energies, normalized on initial values, respectively. Right panel shows EM field energy normalized on its final simulation time value (because it is zero at $t = 0$). The data is for uniform density 3D run.

tric field E_z component at three times. E_z fields show two localized dips with amplitudes of $E_z \approx -5 \times 10^{10}$ V/m that are also spatially co-located with E_x positive and negative electrostatic wakes. Note that in the bottom row of Fig.1 background around the electron bunches appears yellowish color instead of green that corresponds to zero level. This is because of the presence of noise, which in principle can be averaged out to make background green (zero), but this averaging distorts the shape of the two dips in E_z and hence the averaging was not performed.

Fig.2 shows contour plots of logarithm of electron (top row) and ion (bottom row) number densities in (x,y) plane (cut through $z = z_{max}/2$) at different time instants. Here the electron number density includes contributions from background electrons, trailing and driving electron bunches (i.e. all electrons in the simulation). We see that the transverse electric field of the driving bunch expels electrons creating two density cavities with about 50 μm size in y-direction and (1/7)th of x-tick size i.e. $(1.12 - 1.03) \times 10^4/7 \approx 130$ μm size in x-direction. This is consistent with the previous results of Ref.[5]. What is novel however is the inclusion of mobile ions. We see from bottom row panels in Fig.2 that ion density perturbation can be as large as few times the initial ion density and is concentrated in a ion over-density of size 2000 grids which is about 26351 μm.

Fig.3 quantifies the details of background electron, ion, trailing and driving electron bunch distribution functions at different times: open diamonds correspond to $t = 0$, while blue and red curves to the half and the final simulations times, respectively. We gather from the plot that the background electrons develop non-thermal tails in the direction of motion of the trailing and driving electron bunches (i.e. positive x-direction) with values attaining $p_x \approx 3{-}4\, m_e c$. Ions seem to be heated, rather than developing non-thermal tails, which can be witnessed by symmetric broadening of the distribution function. Lower left panel of Fig.3 demonstrates that by end of simulation time the trailing bunch gains energy of 22.4 GeV, starting from initial 20.4 GeV, with an energy transfer efficiencies of 65 percent. The latter is quantified by calculating: (i) The trailing bunch acceleration efficiency

$$AE(t) = \frac{\int_{p_x>p_0}^{\infty} f_{\rm e,TRAILING}(p_x,t)dp_x}{\int_{-\infty}^{\infty} f_{\rm e,TRAILING}(p_x,t=0)dp_x}, \qquad (5)$$

where $p_0 = 1.087587 \times 10^{-17}$ kg m s^{-1} which corresponds to an initial energy of $E_0 = 20.35$ GeV. Note that $p_0/(m_e c) = 39825.1$. Using IDL's `int_tabulated` built-in function that performs five-point Newton-Cotes integration, the values for data of uniform density 3D run are: $AE(t = 0.1744\ {\rm ns}) = 0.6677$, $AE(t = 0.3488\ {\rm ns}) = 0.6674$. (ii) The energy transfer efficiency from the driving bunch to trailing bunch

$$TE(t) = \frac{\int_{p_x>p_0}^{\infty} f_{\rm e,TRAILING}(p_x,t)dp_x}{\int_{-\infty}^{p_0} f_{\rm e,DRIVING}(p_x,t)dp_x}. \qquad (6)$$

The values for data of uniform density 3D run are: $TE(t = 0.1744\ {\rm ns}) = 0.6476$, $TE(t = 0.3488\ {\rm ns}) = 0.6463$. Note that the physical meaning of $AE(t)$ is the fraction of trailing bunch electrons with momenta greater that p_0 (or with energies greater that $E_0 = 20.35$ GeV) of the total number of trailing bunch electrons at $t = 0$. The physical meaning of $TE(t)$ is the fraction of trailing

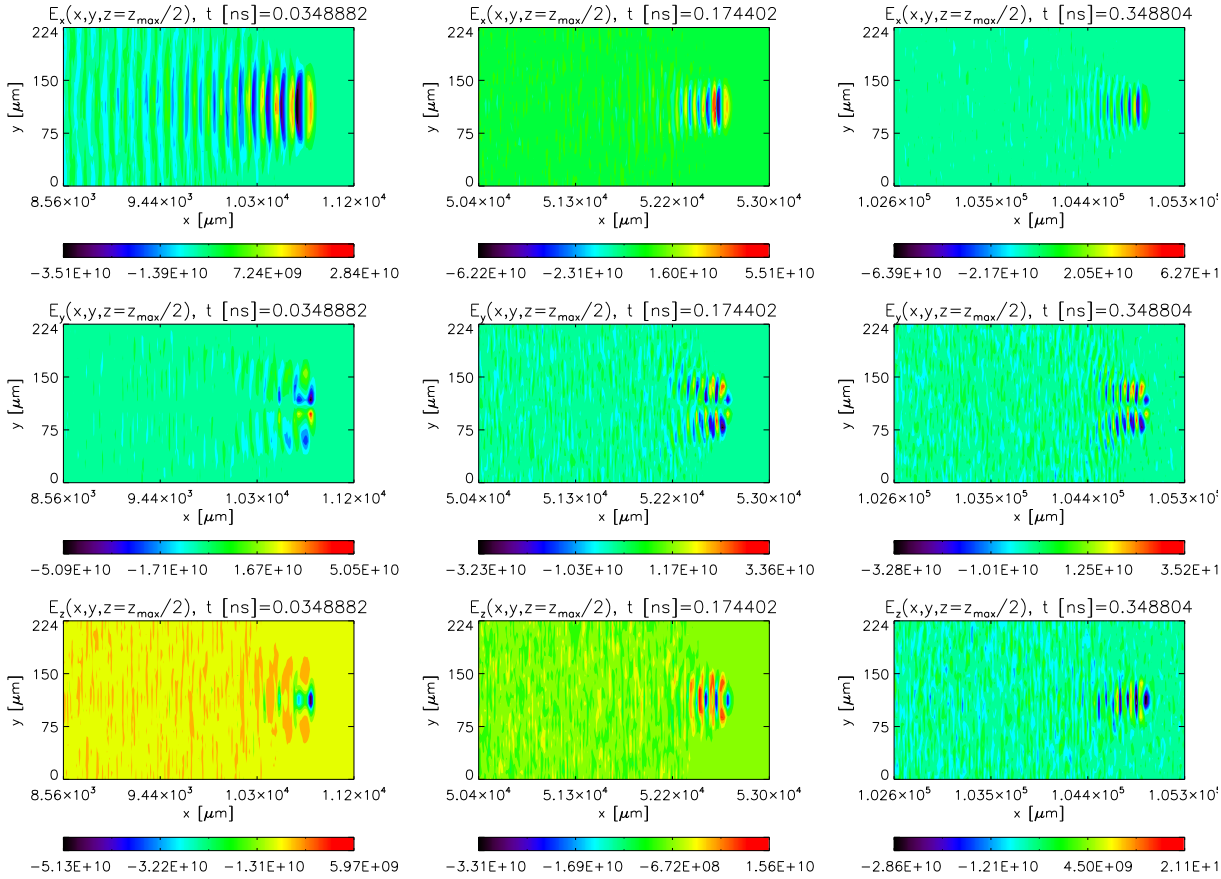

FIG. 5: As in Fig.1 but for the case of positive density gradient, according to equation 1 and 3D.

bunch electrons with momenta greater that p_0 (or with energies greater that $E_0 = 20.35$ GeV) of the number of driving bunch electrons with momenta less than p_0 at time t (not at $t = 0$ – compare the denominators of Equations 5 and 6 and note the different times t used). Because the energy of accelerated trailing bunch electrons comes from the deceleration of driving bunch electrons, the both indexes $AE(t)$ and $TE(t)$ have similar values of 65 percent. Equations 5 and 6 contain infinite integration bounds $\pm\infty$. The employed discretized version has instead bounds of $p_{x,\mathrm{MAX,MIN}} = \pm 1.4 \times 10^{-17}$ kg m s^{-1}. The range was split into 100 million points. Thus calculation of $AE(t)$ and $TE(t)$ indexes is accurate. Lower right panel of Fig.3 demonstrates that by the end of simulation time starting from initial 20.4 GeV, the driving bunch loses energy to about 18.3 GeV.

Left panel of Fig.4 shows the behavior of the total (particles plus EM fields) and particle energies, normalized to initial values, respectively. We see that the total energy increases due to numerical heating, but stays within a tolerable value of 0.065 percent. The particle energy decreases by 0.1 percent. The right panel shows EM field energy normalized to its final simulation time value. We see that it steadily increases as the plasma wake is generated.

B. 3D positive density gradient case

Next we investigate the effect of positive density gradient on PWFA. Fig.5 is similar to Fig.1, but for the case of positive density gradient, according to equation 1 and 3D. We gather from top row of Fig.5 that electrostatic plasma wake becomes spatially localized and, compared to the homogeneous density 3D case, E_x now attains three times larger values of $\pm 6.5 \times 10^{10}$ V/m. This can be explained by the fact that plasma wake size is prescribed by the electron inertial length, c/ω_{pe}. Hence, because of the scaling law $\omega_{pe} \propto \sqrt{n_e}$, the progressively increasing density, into which driving bunch plows through, creates more localized and stronger wake. We also see more oscillations (peaks and troughs) in the wake. This is because the plasma wake is oscillating spatially at ω_{pe}, which is increasing with the increase of number density.

Fig.6 is as in Fig.2 but for the case of positive density gradient, according to equation 1 and 3D. We see that in this case electron density cavities are more compact too, commensurate with a more compact electrostatic

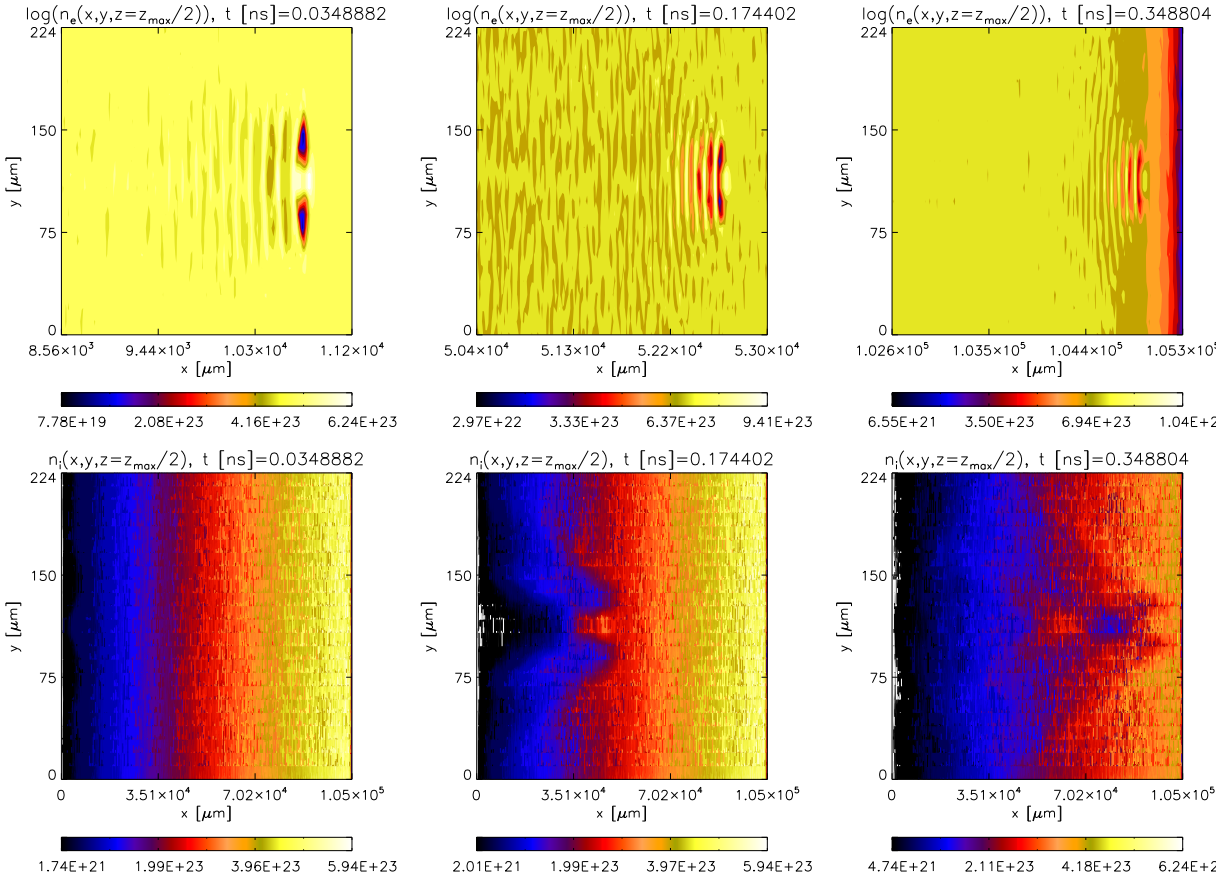

FIG. 6: As in Fig.2 but for the case of positive density gradient, according to equation 1 and 3D.

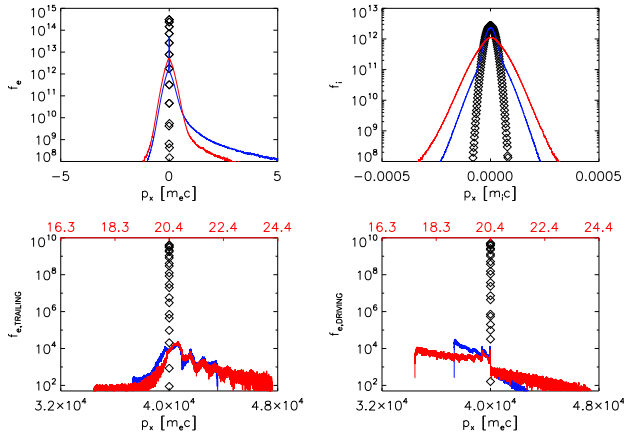

FIG. 7: As in Fig.3 but for the case of positive density gradient, according to equation 1 and 3D.

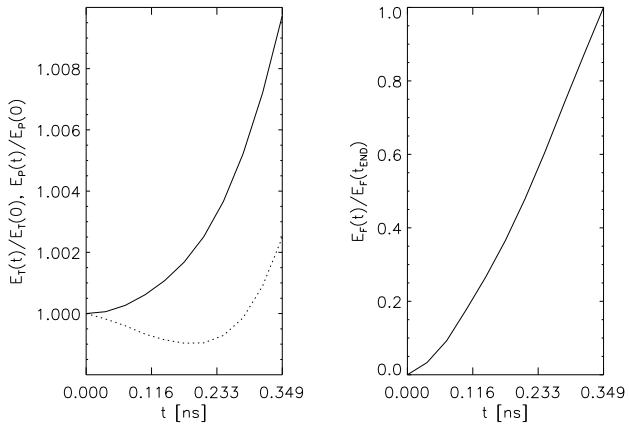

FIG. 8: As in Fig.4 but for the case of positive density gradient, according to equation 1 and 3D.

wake. The blue strip in the rightmost panel of top row in Fig.6 is due to background density falling off to zero, as prescribed by the initial conditions. In the ion density (bottom row) because x-axis spans entire domain, background density 10-fold increase is clearly seen. Ion density perturbation is less profound because it is now on top of the background density 10-fold increase (due to the background density gradient).

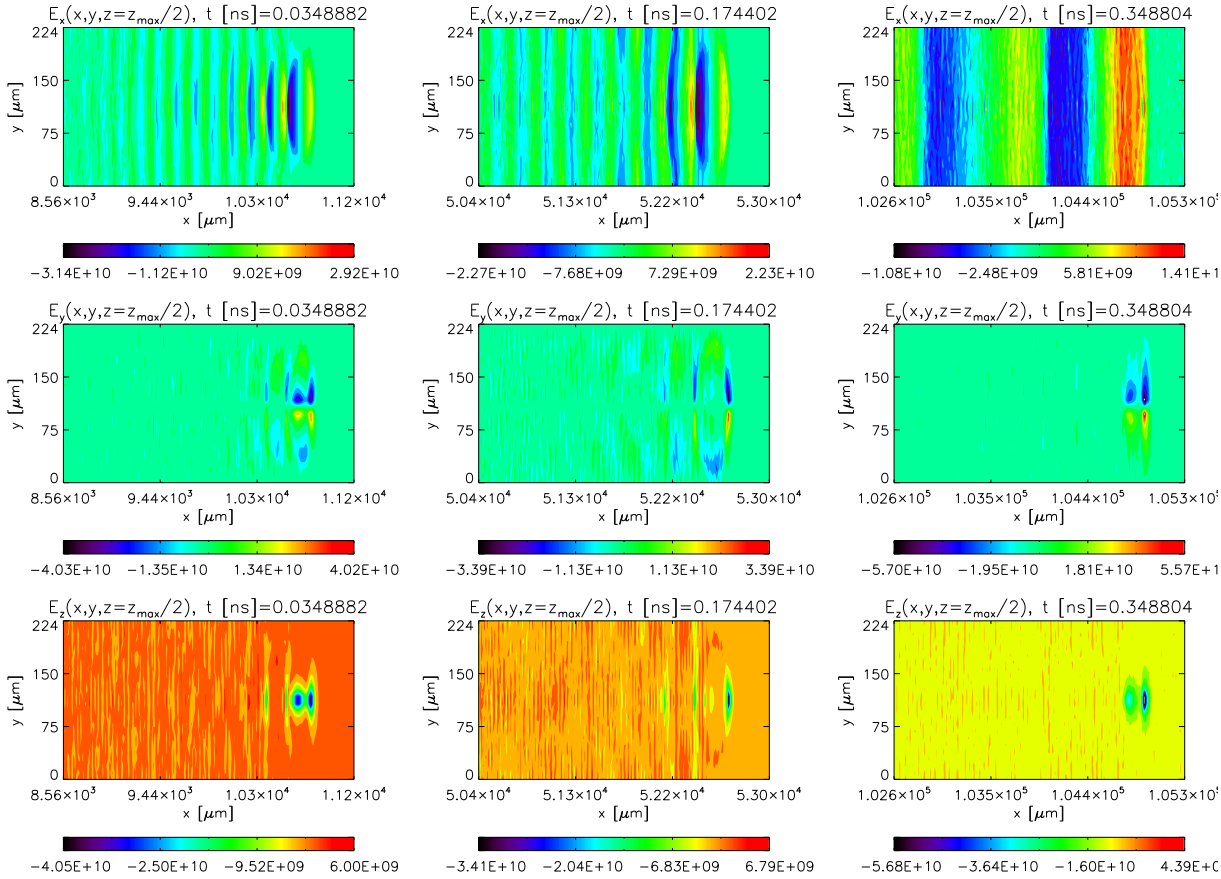

FIG. 9: As in Fig.1 but for the case of negative density gradient, according to equation 2 and 3D.

Fig.7 is as in Fig.3 but for the case of positive density gradient, according to equation 1 and 3D. The top row shows that background electron positive momenta tail is now *intermittently* more energetic, compared to the uniform density 3D case and also ion heating is intermittently more stronger. Bottom left panel shows that trailing bunch energies reach as high as 24.4 GeV. The acceleration and energy transfer efficiencies in this case are calculated as follows: $AE(t = 0.1744\text{ ns}) = 0.6100$, $AE(t = 0.3488\text{ ns}) = 0.7326$ and $TE(t = 0.1744\text{ ns}) = 0.6052$, $TE(t = 0.3488\text{ ns}) = 0.7545$, indicating about 75 percent acceleration and energy transfer efficiency by the end simulation time. The bottom right panel shows that driving bunch partly decelerates and partly accelerates, i.e. red curve now spreads beyond E_0. This can be attributed to re-acceleration of driving bunch due to the positive density gradient. Ref.[8] established that in the case of increasing density along the path of an electron beam wave-particle resonant interaction of Langmuir waves with the beam electrons leads to an efficient particle acceleration. This is because Langmuir waves drift to smaller wavenumbers k, allowing them to increase their phase speed, $V_{ph} = \omega/k$, and, thus, being absorbed by faster electrons. Because we are in the blow out regime, driving beam number density is 2.5 times denser than background electron density, Langmuir waves will grow via bump-on-tail instability on the time scale of $\approx 1/2.5 = 0.4\omega_{pe}^{-1}$. The final simulation time of 0.3488 ns corresponds to $4400\omega_{pe}^{-1}$. Thus there will be a plenty of time for similar effect as in Ref.[8] to take place.

Fig.8 is as in Fig.4 but for the case of positive density gradient, according to equation 1 and 3D. We see that now total energy error is 1 percent. This is larger than in the uniform density 3D case, but still tolerable.

C. 3D negative density gradient case

Next we investigate the effect of negative density gradient on PWFA. Fig.9 is similar to Fig.1, but for the case of negative density gradient, according to equation 2 and 3D. We see in top row of Fig.9 that electrostatic plasma wake becomes spatially wider spread, compared to the homogeneous density 3D case, with larger distances between the peaks and troughs in x-direction. In the transverse y-direction size of the wake grows too, such that by the end of simulation the wake is larger than $y_{max} = 234.229$ μm (note that we plot data up to 23-rd

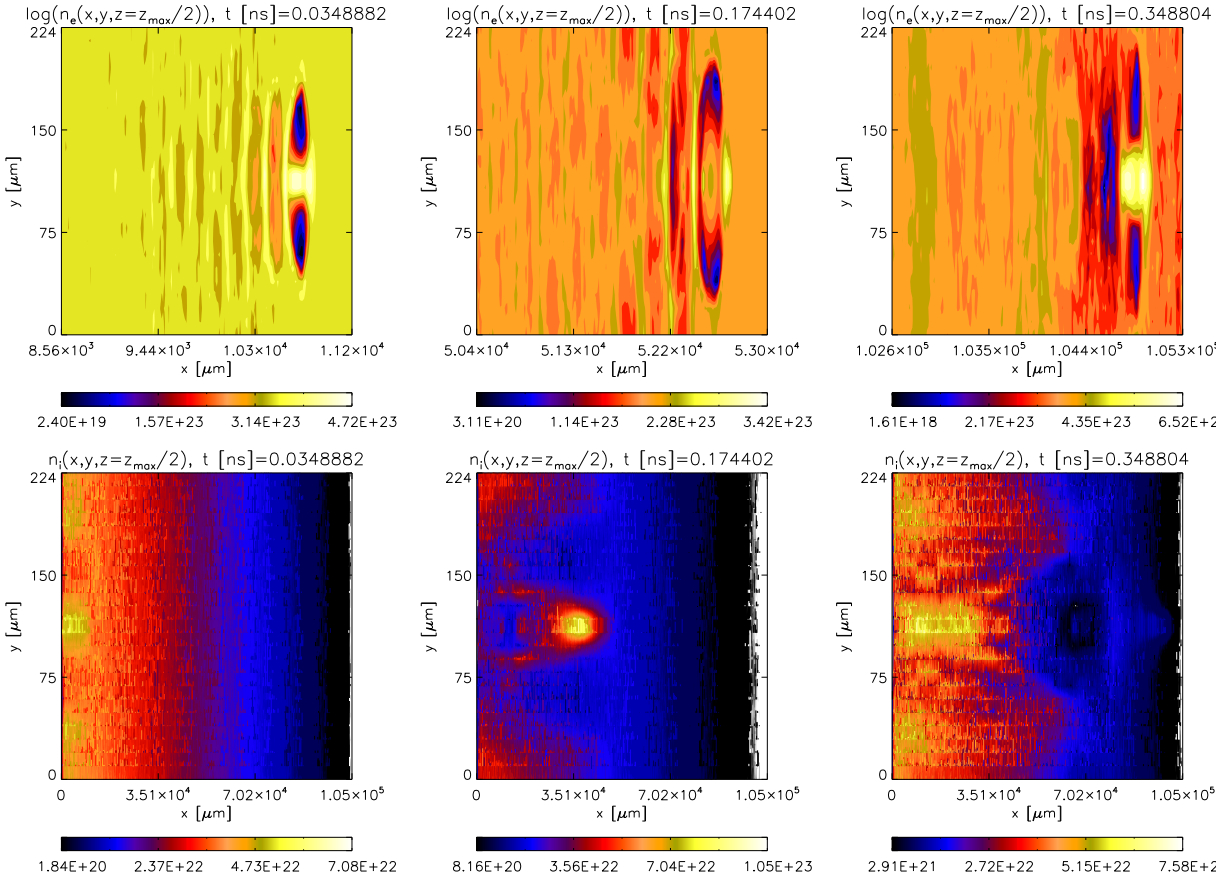

FIG. 10: As in Fig.2 but for the case of negative density gradient, according to equation 2 and 3D.

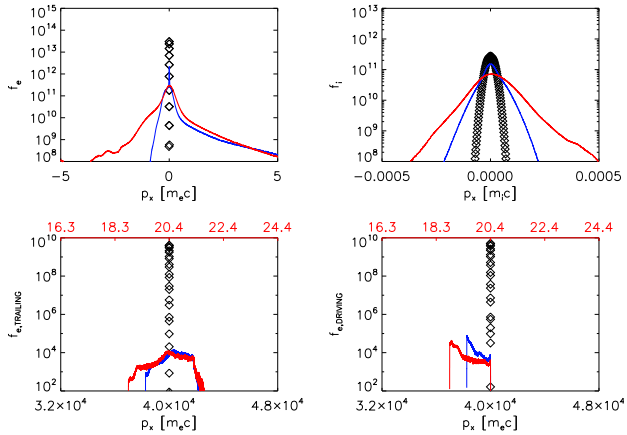

FIG. 11: As in Fig.3 but for the case of negative density gradient, according to equation 2 and 3D.

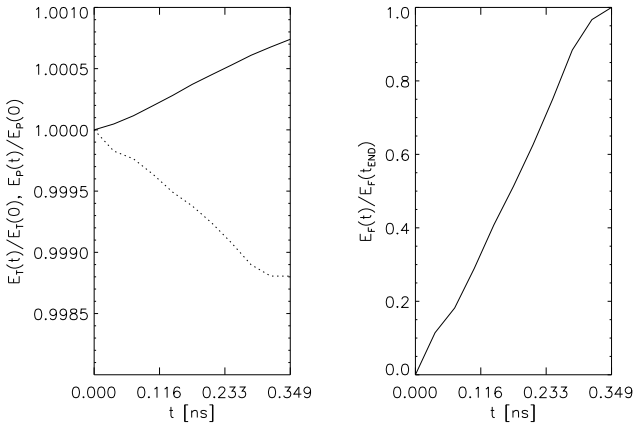

FIG. 12: As in Fig.4 but for the case of negative density gradient, according to equation 2 and 3D.

grid point cutting off plot at 224 μm). E_x now attains two-and-a-half times smaller value of -1.1×10^{10} V/m. Again, this can be explained by the fact that plasma wake size is prescribed by the electron inertial length, $c/\omega_{pe} \propto 1/\sqrt{n_e}$. Thus, progressively decreasing density creates less localized, wider-spread and thus weaker plasma wake. We also see lesser number of oscillations (peaks and troughs) in the wake. This is because the

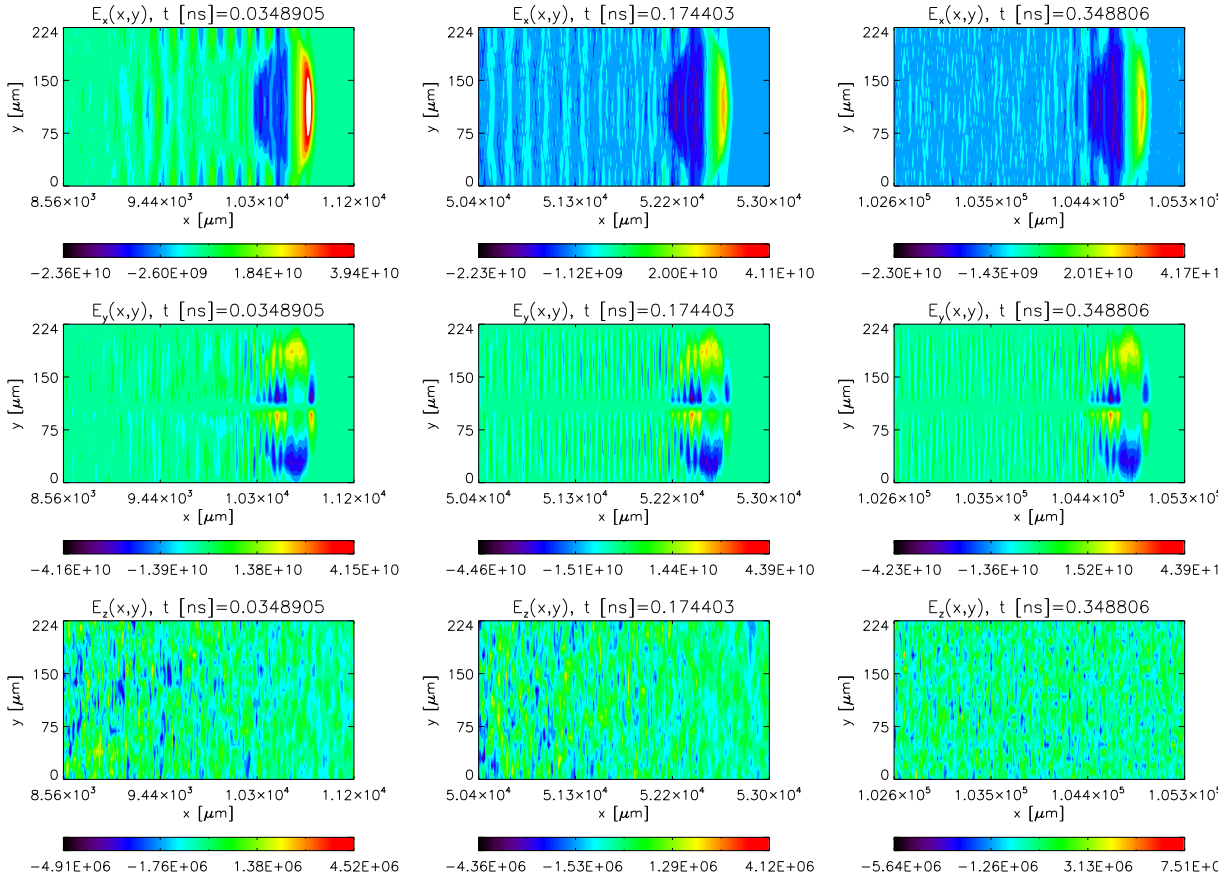

FIG. 13: As in Fig.1 but for the 2D case with uniform density.

plasma wake is oscillating spatially at ω_{pe}, which is decreasing with the decrease of number density. Surprisingly, transverse EM fields (middle and bottom rows in Fig.9) are similar in their structure to that of homogeneous density case (middle and bottom rows in Fig.1). On contrary, in positive density gradient case (middle and bottom rows in Fig.5) we see more localized E_y and E_z. Thus, we conclude that negative gradient affects only electrostatic, E_x component and not E_y or E_z.

Fig.10 is as in Fig.2 but for the case of negative density gradient, according to equation 2 and 3D. We see that in this case electron density cavities are larger in size, commensurate with a more wider-spread electrostatic wake. In the ion density (bottom row) because x-axis spans entire domain, background density 10-fold decrease is clearly seen. Ion density perturbation is of the same order as the background density.

Fig.11 is as in Fig.3 but for the case of negative density gradient, according to equation 2 and 3D. The top row shows that background electron positive momenta tail is now more energetic compared to the uniform density 3D case and also ion heating is more stronger. The bottom left panel shows that trailing bunch energies reach only 21.4 GeV. The acceleration and energy transfer efficiencies in this case are calculated as follows: $AE(t = 0.1744\text{ ns}) = 0.6187$, $AE(t = 0.3488\text{ ns}) = 0.4617$ and $TE(t = 0.1744\text{ ns}) = 0.6004$, $TE(t = 0.3488\text{ ns}) = 0.4465$, indicating 45 percent acceleration and energy transfer efficiency by the end simulation time. The bottom right panel shows that driving bunch only decelerates i.e. blue and red curves shifts to the left of E_0.

Fig.12 is as in Fig.4 but for the case of negative density gradient, according to equation 2 and 3D. We see that now total energy error is 0.065 percent, which is similar to the uniform density 3D case.

D. 2D homogeneous density case

We now investigate the effect of dimensions of the system on PWFA. Fig.13 is similar to Fig.1, but for the case of uniform density and 2D. We infer from top row of Fig.13 that electrostatic plasma wake is similar to the 3D uniform density case both in terms of morphological structures (positive and negative half ellipses) and values attained of -2.3×10^{10} V/m. The same is true for the transverse y-direction, except that in addition to quadrupolar structure of E_y seen in 3D, two opposite

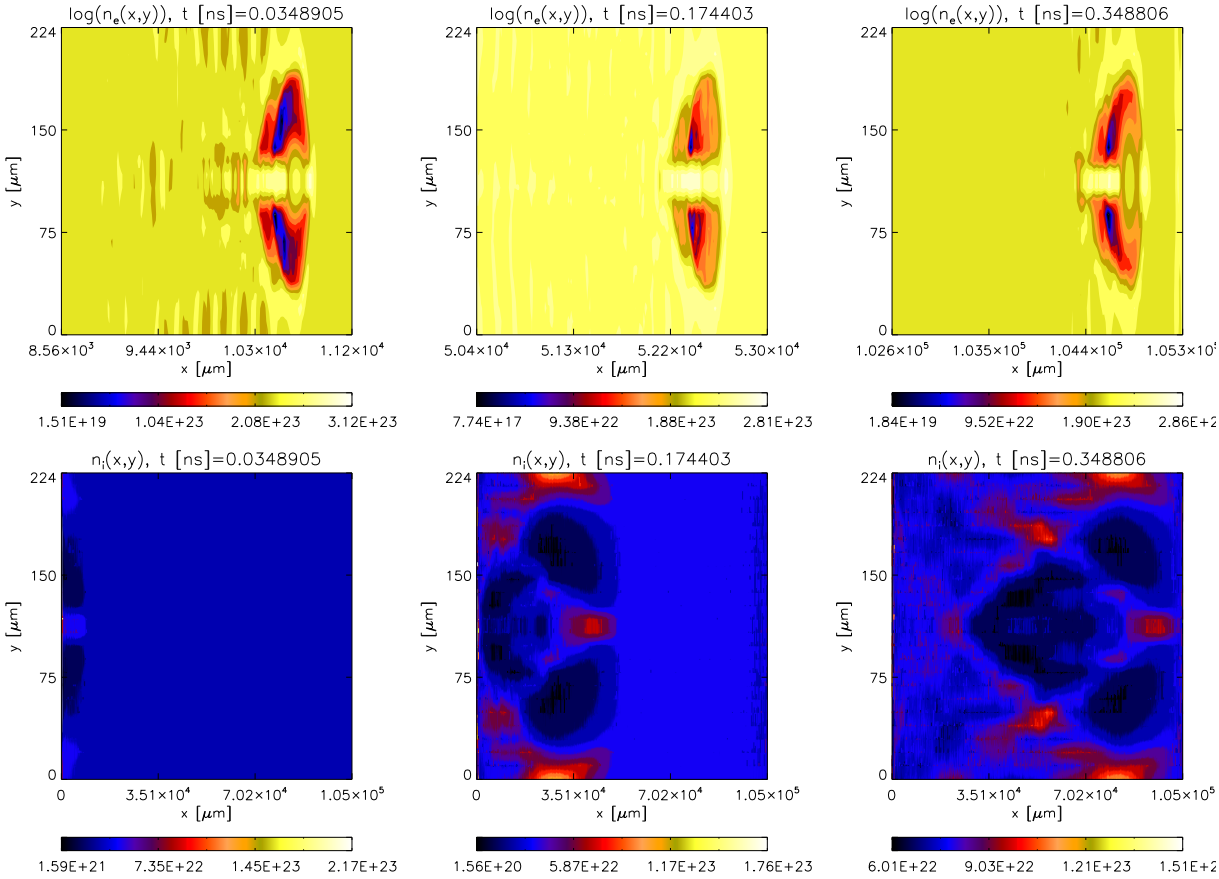

FIG. 14: As in Fig.2 but for the 2D case with uniform density.

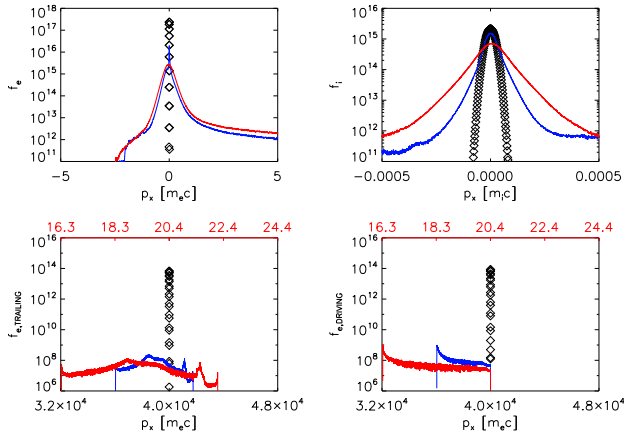

FIG. 15: As in Fig.3 but for the 2D case with uniform density.

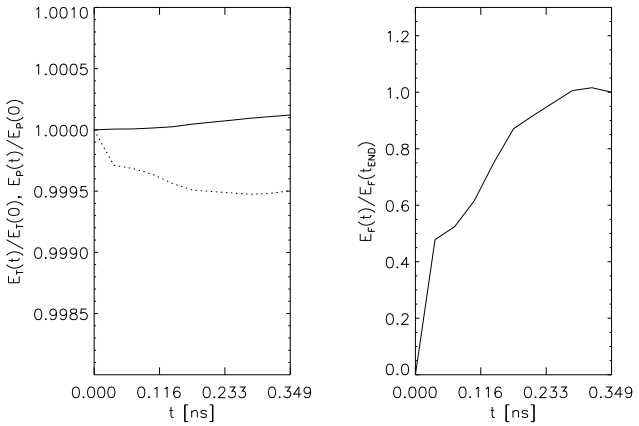

FIG. 16: As in Fig.4 but for the 2D case with uniform density.

polarity lobes appear further away from symmetry axis. The attained values of $E_y \approx \pm 4.3 \times 10^{10}$ V/m are also similar to 3D case. There is a marked difference in the transverse z-direction. Because, z is now ignorable direction in 2D simulation, no relative displacement of ions and electrons is possible. Thus, E_z plot remains featureless and at a noise level.

Fig.14 is as in Fig.2 but for the case of uniform density and 2D. We see that in this case electron density cavities

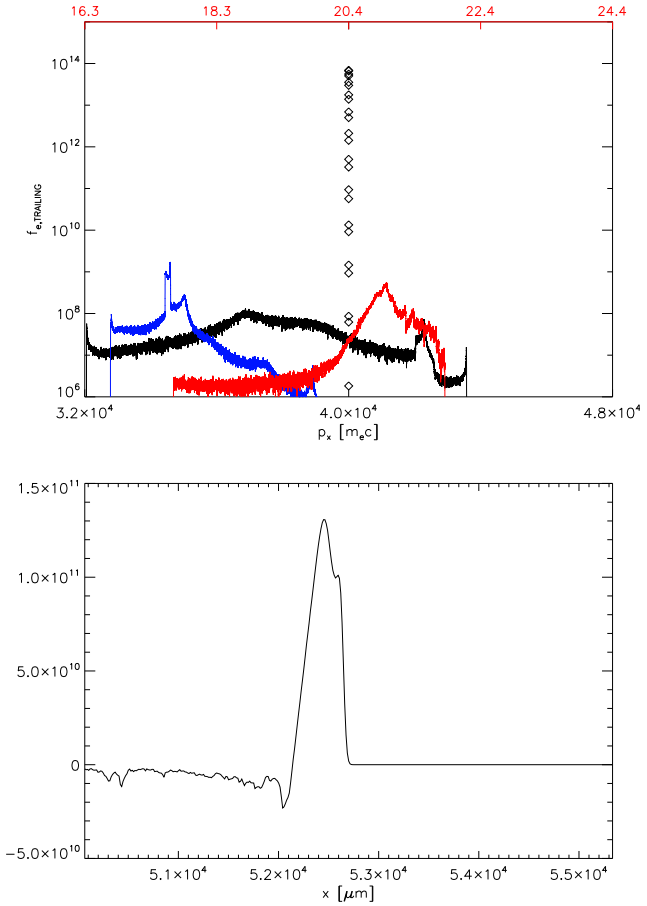

FIG. 17: Top panel is similar to lower left panel of Fig.3, in that it shows trailing electron bunch distribution functions at different times: open diamonds at $t = 0$, while (i) black, (ii) blue and (iii) red curves here all correspond to the final simulation time for (i) uniform density, (ii) negative and (iii) positive density gradients in 2D cases. Bottom panel is $E_x(x)$ profile at middle simulation time ($t = 0.1744$ ns) in 1D case.

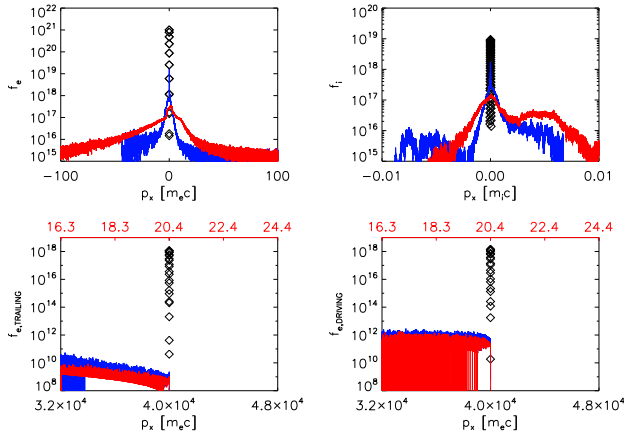

FIG. 18: As in Fig.3 but for the 1D case with uniform density.

are larger in size. In the ion density (bottom row) density perturbations are less profound and show more complex structuring.

Fig.15 is as in Fig.3 but for the case of uniform density and 2D. The top row shows that background electron positive momenta tail is now very energetic compared to the uniform density 3D case and also ion heating is more stronger. Bottom left panel shows that trailing bunch energies reach only 22.4 GeV. The acceleration and energy transfer efficiencies in this case are calculated as follows: $AE(t = 0.1744\text{ ns}) = 0.0989$, $AE(t = 0.3488\text{ ns}) = 0.0992$ and $TE(t = 0.1744\text{ ns}) = 0.0957$, $TE(t = 0.3488\text{ ns}) = 0.0963$, indicating 10 percent acceleration and energy transfer efficiency by the end simulation time. The bottom right panel shows that driving bunch decelerates stronger in the 2D case, compared to 3D, i.e. red curve moves further to the left of E_0.

Fig.16 is as in Fig.4 but for the case of uniform density and 2D. We see that because we used about 11 times more particles per simulation cell, now total energy error is 0.01 percent, which is much smaller compared to the uniform density 3D case.

E. Comparison of 2D density gradient and uniform cases and 1D homogeneous density case

We start this subsection by presenting a comparison of 2D positive and negative density gradient and uniform cases. Top panel of Fig.17 is analogous to lower left panel of Fig.3, in that it shows trailing electron bunch distribution functions at different times: open diamonds are for $t = 0$, while (i) black, (ii) blue and (iii) red curves here correspond to final simulation time for (i) uniform density, (ii) negative and (iii) positive density gradient cases in 2D. We gather that positive gradient results in more efficient trailing bunch acceleration as the red curve has larger peak than the black curve. The blue curve is located entirely to left of E_0 indicating no acceleration at all for the negative gradient case. This is in stark contrast to 3D negative gradient case (lower left panel of Fig.11) where 45 percent efficient trailing bunch acceleration was witnessed. The acceleration and energy transfer efficiencies in this case are calculated as follows: $AE(t = 0.3488\text{ ns}) = 0.0993$ (black curve, uniform density), $AE(t = 0.3488\text{ ns}) = 7.739\times10^{-7}$ (blue curve, negative gradient), $AE(t = 0.3488\text{ ns}) = 0.7859$ (red curve, positive gradient), and $TE(t = 0.3488\text{ ns}) = 0.0963$ (black curve, uniform density), $TE(t = 0.3488\text{ ns}) = 7.501\times10^{-7}$ (blue curve, negative gradient), $TE(t = 0.3488\text{ ns}) = 0.7808$ (red curve, positive gradient), indicating the following acceleration and energy transfer efficiency by end simulation time: 10 percent for uniform density, negligible (zero) for negative gradient and 78 percent for positive gradient cases. Thus we conclude that two-dimensional simulation results are substantially different from the three-dimensional ones.

The bottom panel of Fig.17 is $E_x(x)$ profile at mid-

dle simulation time in 1D case. We see that no substantial negative electrostatic wake follows the positive peak. This is because in 1D no transverse electric field can be sustained (because transverse directions are ignorable) and thus the driving bunch cannot expel electrons to create density cavities.

Fig.18 is as in Fig.3 but for the 1D case with uniform density. We learn from the figure that the background electrons and ions show extreme levels of superthermal particle tails (note the 20-fold increase in the x-axis range in the top row). The bottom row of Fig.18 demonstrates that both trailing and driving bunches are decelerated, as both blue and red curves stay below the initial bunch energy of E_0. For completeness we calculated the acceleration and energy transfer efficiencies as follows: $AE(t = 0.3488\,\text{ns}) = 6.904 \times 10^{-7}$ and $TE(t = 0.3488\,\text{ns}) = 6.732 \times 10^{-7}$, indicating negligible (zero) acceleration and energy transfer efficiency by the end simulation time.

III. CONCLUSIONS

We have carried out 3D, 2D and 1D, particle-in-cell, fully electromagnetic simulations of electron plasma wake field acceleration in the blow out regime. Our aim was to extend earlier results of Ref.[5] by (i) studying the effect of longitudinal density gradient in the light of the results of Ref.[8]; (ii) avoiding use of co-moving simulation box because the density gradient cases require considering a long domain that fits the entire gradient; (iii) inclusion of ion motion; and (iv) studying fully electromagnetic plasma wake fields without quasi-static approximation of QuickPIC [3]. We have shown that injecting driving and trailing electron bunches into a positive density gradient of ten-fold increasing density over 10 cm long plasma, results in spatially more compact and three times larger electric fields (-6.4×10^{10} V/m), leading to acceleration of the trailing bunch up to 24.4 GeV (starting from initial 20.4 GeV), with an energy transfer efficiencies from leading to trailing bunch of 75 percent compared to the uniform density case. In the latter case -2.5×10^{10} V/m wave is created leading to acceleration of the trailing bunch up to 22.4 GeV, with an energy transfer efficiencies of 65 percent. We have shown that injecting the electron bunches into a negative density gradient of ten-fold decreasing density over 10 cm plasma, yields spatially more spread wake and two-and-half smaller electric fields (-1.0×10^{10} V/m), leading to a weaker acceleration of the trailing bunch up to 21.4 GeV (starting from initial 20.4 GeV), with an energy transfer efficiencies from leading to trailing bunch of 45 percent. We have shown that 2D simulation results are substantially different from the 3D ones, showing only 10 percent efficiency of trailing bunch acceleration, while in 1D case no acceleration is seen. We included ion motions into consideration showing that in the plasma wake ion number density can increase over few times the background value. Finally, we also show that transverse electromagnetic fields in plasma wake are of the same order as the longitudinal (electrostatic) ones.

In terms of an experimental implementation of the proposed PWFA experiments with the longitudinal density gradient, we would like to remark the following: (i) The positive density gradient maybe created by driving a hollow piston in the photo-ionized Lithium vapor plasma contained in heat-pipe oven [7], as in FACET [2]. The 10-fold compression of the plasma density may be created by the piston moving in the same direction as the driving and trailing electron bunches that would fly through a hole in the piston. (ii) The negative density gradient, e.g. a 10-fold rarefaction, maybe created by pulling the hollow piston the opposite direction to the bunch's motion through a hole in the piston.

Acknowledgments

Author is financially supported by Leverhulme Trust Research Project Grant RPG-311. This research utilized Queen Mary University of London's (QMUL) MidPlus computational facilities, supported by QMUL Research-IT and funded by UK EPSRC grant EP/K000128/1. EPOCH code development work was in part funded by the UK EPSRC grants EP/G054950/1, EP/G056803/1, EP/G055165/1 and EP/ M022463/1.

[1] T.D. Arber and et al. Plasm. Phys. Contr. Fus., **57**, 1, (2015), doi:10.1088/0741-3335/57/11/113001.
[2] M.J. Hogan and et al. New J. Phys., **12**, 055030, (2010), doi:10.1088/1367-2630/12/5/055030.
[3] C. Huang and et al. J. Phys. Conf. Ser., **46**, 190, (2006), doi:10.1088/1742-6596/46/1/026.
[4] W.D. Kilpatrick. Rev. Sci. Instr., **28**, 824, (1957), doi:10.1063/1.1715731.
[5] M. Litos and et al. Nature, **515**, 92, (2014), doi:10.1038/nature13882.
[6] J.L. Miller. Phys. Today, **68 (1)**, 11, (2015), doi:10.1063/PT.3.2639.
[7] P. Muggli and et al. IEEE Trans. Plasm. Sci., **27**, 791, (1999), doi:10.1109/27.774685.
[8] R. Pechhacker and D. Tsiklauri. Phys. Plasmas, **21**, 012903, (2014), doi:10.1063/1.4863494.